Circulation: Cardiovascular Imaging

ORIGINAL ARTICLE

Diagnostic Accuracy of a Machine-Learning Approach to Coronary Computed Tomographic Angiography–Based Fractional Flow Reserve

Result From the MACHINE Consortium

See Editorial by Min
See Editorial by Yeri and Shah

Adriaan Coenen, MD
Young-Hak Kim, MD, PhD
Mariusz Kruk, MD, PhD
Christian Tesche, MD
Jakob De Geer, MD, PhD
Akira Kurata, MD, PhD
Marisa L. Lubbers, MD
Joost Daemen, MD, PhD
Lucian Itu, PhD
Saikiran Rapaka, PhD
Puneet Sharma, PhD
Chris Schwemmer, MS
Anders Persson, MD, PhD
U. Joseph Schoepf, MD
Cezary Kepka, MD, PhD
Dong Hyun Yang, MD, PhD
Koen Nieman, MD, PhD

BACKGROUND: Coronary computed tomographic angiography (CTA) is a reliable modality to detect coronary artery disease. However, CTA generally overestimates stenosis severity compared with invasive angiography, and angiographic stenosis does not necessarily imply hemodynamic relevance when fractional flow reserve (FFR) is used as reference. CTA-based FFR (CT-FFR), using computational fluid dynamics (CFD), improves the correlation with invasive FFR results but is computationally demanding. More recently, a new machine-learning (ML) CT-FFR algorithm has been developed based on a deep learning model, which can be performed on a regular workstation. In this large multicenter cohort, the diagnostic performance ML-based CT-FFR was compared with CTA and CFD-based CT-FFR for detection of functionally obstructive coronary artery disease.

METHODS AND RESULTS: At 5 centers in Europe, Asia, and the United States, 351 patients, including 525 vessels with invasive FFR comparison, were included. ML-based and CFD-based CT-FFR were performed on the CTA data, and diagnostic performance was evaluated using invasive FFR as reference. Correlation between ML-based and CFD-based CT-FFR was excellent (R=0.997). ML-based (area under curve, 0.84) and CFD-based CT-FFR (0.84) outperformed visual CTA (0.69; P<0.0001). On a per-vessel basis, diagnostic accuracy improved from 58% (95% confidence interval, 54%–63%) by CTA to 78% (75%–82%) by ML-based CT-FFR. The per-patient accuracy improved from 71% (66%–76%) by CTA to 85% (81%–89%) by adding ML-based CT-FFR as 62 of 85 (73%) false-positive CTA results could be correctly reclassified by adding ML-based CT-FFR.

CONCLUSIONS: On-site CT-FFR based on ML improves the performance of CTA by correctly reclassifying hemodynamically nonsignificant stenosis and performs equally well as CFD-based CT-FFR.

Key Words: area under curve ■ computed tomography angiography ■ coronary artery disease ■ hemodynamics ■ machine learning

http://circimaging.ahajournals.org

CLINICAL PERSPECTIVE

The diagnostic performance of coronary computed tomographic angiography (CTA) to detect functional relevant coronary artery disease can be improved by adding computational fluid dynamics onto the anatomic CTA information (CT-fractional flow reserve [FFR]). The diagnostic performance of a machine-learning approach was compared with computational fluid dynamics–based CT-FFR and CTA, and all were validated against invasive FFR. In this multicenter registry, 351 patients, 525 vessels were investigated. In this study, 299 of the 525 vessels (57%) had a physiologically intermediate stenoses (invasive FFR between 0.70 and 0.90), indicating a challenging clinically relevant population. Per-vessel accuracy of machine-learning– and computational fluid dynamics–based CT-FFR were similar (both 78%), and both outperformed standard conventional CTA evaluation (58%). On a per-patient level, diagnostic performance of machine-learning–based CT-FFR was significantly larger for the tertile with the highest image quality (91%) compared with the tertile with the lowest image quality (75%). Diagnostic performance of CTA can be improved with machine-learning–based CT-FFR, potentially reducing the number of unnecessary referrals for invasive coronary angiography. Image quality remains important even with the introduction of CT-FFR technology.

Coronary computed tomographic angiography (CTA) has become a reliable modality for the detection of coronary artery disease (CAD).[1,2] Current guidelines recommend CTA in the work-up for patients with stable chest pain and a low-intermediate probability of obstructive CAD.[3,4] However, many coronary CTA examinations reveal intermediate coronary artery stenosis, and functional assessment of these lesions is critical for meaningful management decision making. Invasively measured fractional flow reserve (FFR) is generally regarded as the clinical standard for lesion-specific assessment of hemodynamic significance.[3,5,6]

Using computational fluid dynamics (CFD), a virtual FFR can be calculated from coronary CTA images (CT-FFR), which shows good correlation with invasively measured FFR and improves the diagnostic performance of coronary CTA alone.[7–11] In addition, computationally less intensive CT-FFR applications, which can be performed locally on regular workstations, have been introduced.[12–17]

Most recently, computational FFR applications based on machine-learning (ML) have been developed. Previously, ML applications were used in both cardiovascular and general medical imaging.[18–24] Contrary to the CFD approach, virtual FFR based on ML applies a combination of pattern recognition and computational learning to derive FFR. In this multicenter collaboration, we evaluated the diagnostic performance of a new ML-based CT-FFR algorithm.

METHODS

Design

The data, analytic methods, and study materials will not be made available to other researchers for purposes of reproducing the results or replicating the procedure. The MACHINE consortium (Machine Learning Based CT Angiography Derived FFR: A Multi-Center Registry) is a collaboration between 5 institutions in North-America, Europe, and Asia, created to investigate the performance of ML-based CT-FFR (URL: https://www.clinicaltrials.gov. Unique identifier: NCT02805621). Each participating center previously evaluated the diagnostic performance of the first-generation on-site CT-FFR application based on CFD and reported results in a peer-reviewed publication.[13–16,25] The patient cohorts and CT data from these studies form the basis for the current study. Approval by the medical ethics committee was obtained at each of the centers. Two sites obtained written informed consent from all patients,[14,16] and at the remaining 3 sites, the local medical ethics committee provided a waiver for the informed consent because of the retrospective study design.[13,15,25]

Population

Respective study cohorts were prospectively recruited at 1 site[14] and retrospectively identified based on the availability of CTA and invasive FFR measurements at the 4 other sites.[13,15,16,25] From the 417 initially identified patients, 65 (16%) were excluded, leaving a total study population of 352 patients (Figure 1). A detailed description of the recruitment and exclusion criteria per center is available in Table 1. In a single patient (2 vessels), the ML-based CT-FFR application could not compute a CT-FFR, thus leaving 351 patients and 525 vessels with invasive FFR measurements for direct comparison.

Coronary CTA

All CT scans were performed on first- and second-generation dual-source CT scanners (Somatom Definition or Somatom Definition Flash; Siemens Healthcare GmbH, Forchheim, Germany). All scans were reconstructed using a medium-smooth kernel and a slice thickness ≤0.75 mm with an increment of 0.4 mm. β-Blockers were administered in patients with high heart rates, and sublingual nitroglycerin was given routinely in 4 centers (299 patients). The mean radiation dose of the CTA examinations was 8.3±6.0 mSv (Table 2). The CTAs were evaluated by observers with extensive previous experience in cardiac imaging. All vessels of interest were classified following the Society of Cardiovascular Computed Tomography criteria: normal: 0% stenosis; minimal: <25% stenosis; mild: 25% to 49% stenosis; moderate: 50% to 69% stenosis; severe: 70% to

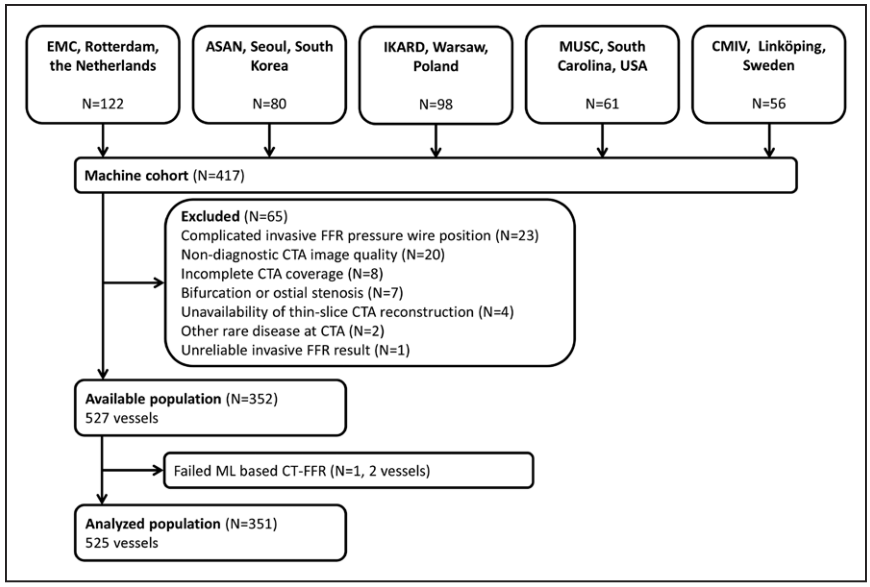

Figure 1. Inclusion flowchart.
Patient selection per site is further described in Table 1. CTA indicates computed tomographic angiography; FFR, fractional flow reserve; and ML, machine-learning.

99%; and occluded: 100%.[26] Any stenosis deemed ≥50% was considered angiographically significant. Image quality was subjectively classified per patients using a 4-point Likert score (1 nondiagnostic; 2 poor impaired image quality, differentiation of the coronary artery wall possible with reduced confidence; 3 adequate, reduced image quality because of artifacts without limiting coronary artery wall differentiation; and 4 excellent, no artifacts present and clear differentiation of the coronary artery wall). In 314 patients, a calcium scan was performed.

Table 1. Detailed Inclusion and Exclusion Per Center

Center	Inclusion Period	Maximum CTA-FFR Interval	Patients/Vessels Included	Exclusion Criteria*	Technical Exclusions
EMC (25)	January 2007–December 2013	50 d	116/203		6 (5%): insufficient CTA quality (4), incomplete CTA coverage (2)
ASAN (16)	December 2011–October 2014	48 d	72/138	Chronic total occlusions, Agatston score >3000, misalignment artifacts	8 (10%): insufficient CTA quality (8)
IKARD (14)	January 2013–December 2014	6 mo	90/96	Unstable angina, atrial fibrillation, body mass index >40	8 (8%): incomplete CTA coverage (6), complicated invasive FFR pressure wire position matching (2)
MUSC (13)	September 2008–November 2013	3 mo	53/67	Bifurcation lesions type D or G, major cardiac event between procedures, severely reduced left ventricle function, stenosis in the proximal left or right coronary artery, chronic total occlusion	8 (13%): bifurcation stenosis (5), insufficient CTA quality (3)
CMIV (15)†	September 2009–March 2012	120 d	21/23	Ostial stenosis	35 (63%): complicated invasive FFR pressure wire position matching (21), insufficient CTA image quality (5), absence of thin-slice CTA reconstructions (4). other cardiovascular conditions (2), ostial stenosis (2), unreliable invasive FFR result (1)

Inclusion of patients per center. In total, 417 patients were identified (included+excluded patients) in all centers. The main reasons for exclusion were problematic matching of invasive FFR pressure wire position (23) and the CTA image quality (20). ASAN indicates Asan Medical Center. Seoul, South Korea; CMIV, Center for Medical Image Science and Visualization, Linköping, Sweden; CTA, computed tomography angiography; EMC, Erasmus Medical Center, Rotterdam, the Netherlands; FFR, fractional flow reserve; IKARD, Instytut Kardiologii, Warsaw, Poland; and MUSC, Medical University of South Carolina, South Carolina, USA.

*On top of exclusion criteria used by all centers: previous coronary artery bypass graft, previous percutaneous coronary intervention, previous myocardial infarction in the vessel investigated by invasive FFR.

†CMIV excluded an additional 7 patients because of a previous surgery/vascular intervention, and these are not mentioned explicitly here as for the other 4 sites, these patients were not included.

Table 2. Patients Characteristics

No. of patients, n	351
Age, y	62.3±9.3
Male sex, n (%)	258 (74)
Body mass index, kg/m²*	27±3.9
Cardiovascular risk factors, n (%)	
Hypertension	232 (66)
Dyslipidemia	210 (60)
Diabetes mellitus	75 (21)
Family history of CAD	119 (34)
Smoking within the last year	120 (34)
Prior myocardial infarction, n (%)†	22 (6)
Prior percutaneous coronary intervention, n (%)†	53 (15)
Heart rate during CTA	64±10
CTA effective radiation dose, mSv	8.3±6.0
Agatston coronary calcium score‡	289 (39–679)
CTA image quality§	3.3±0.5

Values are reported as mean±SD or absolute number n and percentage (%). CAD indicates coronary artery disease; CTA, computed tomography angiography; and FFR, fractional flow reserve.

*Not available in 9 patients.

†Not in the vessel territories interrogated by invasive FFR.

‡Not available in 37 patients, represented in median and (interquartile).

§Based on a 4-point Likert scale (1 nondiagnostic; 2 impaired image quality, differentiation of the coronary artery wall possible with reduced confidence; 3 adequate, reduced image quality because of artifacts without limiting coronary artery wall differentiation; and 4 excellent, no artifacts present, and clear differentiation of the coronary artery wall).

CFD based CT-FFR

At each center, all cases were reevaluated with the latest iteration of a CT-FFR application using CFD (cFFR version 1.4, Siemens Healthcare GmbH). With the observer blinded to all other test results, the coronary artery tree was isolated semi automatically to generate a 3-dimensional (3D) coronary model. All vessels and side branches with a vessel diameter of at least 1.5 mm were included as far as image quality allowed. Generation of the 3D coronary model took ≈30 to 60 minutes per case.[13–16,25] The exact same 3D segmentation models were used to compute both the CFD- and ML-based CT-FFR values. CT-FFR values were recorded at identical locations within the vessel for both the CFD and ML CT-FFR approaches. The on-site CFD application in this study, which is described in detail elsewhere,[27] is a hybrid CFD approach that couples a reduced-order model for nonstenotic vessel sections with a dedicated stenosis model for the narrowed regions. One of the main presumptions behind this approach is that within the nonstenotic regions, the changes in intracoronary blood pressure (or FFR) are small and thus do not require elaborate computation.[25] Although the hybrid CFD application is relatively time efficient, solving the CFD equations throughout the coronary artery tree is a computational-intensive procedure and takes up to 10 minutes on a workstation PC. Coronary flow and pressure are simulated both at rest and in a hyperemic state by virtual reduction of the microvascular resistance, thereby simulating the effect of adenosine infusion.[28] The intracoronary blood pressure in the hyperemic state is then divided by the blood pressure in the aorta, similar to invasive FFR, and displayed as a color-coded map onto the 3D coronary model.[25,27]

ML based CT-FFR

The CT-FFR application in this study was developed using a supervised learning approach, which implies that the ML algorithm based on anatomic features was trained against a ground truth. As described in the original article by Itu et al,[29] the ML application was trained using 12 000 synthetic 3D coronary models of various anatomy and degrees of CAD, for which the CFD-based CT-FFR values were computed. The CFD-based results from the 12 000 synthetic coronary models were used as the ground truth training data for the ML-based CT-FFR application. The ML-based CT-FFR model was trained using a deep learning model to integrate the complex nonlinear relationship between the various features extracted from the coronary tree geometry. The model is based on 28 input features (Table I in the Data Supplement), that is, 28 variables that were extracted for each 3D geometry to learn their relationship to the CFD-based CT-FFR values. The interactions between these 28 features are modeled in a neural network.[29]

For the current validation study, CFD-based CT-FFR and the ML-based CT-FFR were independently performed but using the same coronary models segmented from the CT scan. Also, the same FFR sampling locations were used to derive both the CFD- and ML-based CT-FFR values (cFFR version 2.1, Siemens Healthcare GmbH; currently not commercially available).

Invasive Coronary Angiography and FFR

Invasive coronary angiography (ICA) was performed following local standards. Invasive FFR was either performed for clinical reasons or for research purposes. An FFR pressure wire was positioned distal to the stenosis of interest, after which hyperemia was induced by intravenous infusion of adenosine at 140 μg/kg per minute. FFR values ≤0.80 were considered hemodynamically significant. To coregister the location of invasive FFR measurement and CTA-FFR, an independent observer without knowledge of angiographic or functional results identified the invasive FFR sample location on fluoroscopy images and registered the corresponding location as an anatomic landmark.

Statistics

Absolute variables are represented as totals and percentages, continuous variables as means and SDs (±) or medians and interquartile ranges. Effective radiation dose was calculated using a conversion factor of 0.014 (mSv/mGy per centimeter). Correlations between ML- and CFD-based CT-FFR and invasive FFR were calculated with the Pearson correlation coefficient. C statistics were calculated for ML and CFD CT-FFR and visual CTA and compared by using the method of DeLong et al.[30]

CTA was investigated both using a threshold of 50% and 70% lumen diameter reduction. For both ML- and CFD-based CT-FFR, a value ≤0.80 was regarded as hemodynamically significant. These classifications were compared with invasive FFR applying the same threshold of ≤0.80 for a functionally obstructive coronary artery stenosis. Diagnostic performance was reported on a per-vessel basis as sensitivity, specificity, positive predictive value, negative predictive value, and accuracy, for all vessels investigated with invasive FFR comparison.

The 95% confidence intervals (CIs) were corrected for within patient clustering of data using generalized estimating equations.[31] A nonoverlapping 95% CI was used to determine statistical significance.

In addition, a per-patient analysis was performed, which included vessels without direct FFR confirmation. Based on available findings, independent, blinded reviewers assessed the per-patient presence of hemodynamically significant CAD. For the invasive reference: based on the hierarchical presence of FFR ≤0.80 or ICA stenosis >90%, vessels were considered to have hemodynamically significant CAD. If the FFR was >0.80 or stenosis severity by ICA was <50%, vessels were classified as not significantly diseased. Patients with a 50% to 90% stenosis at ICA and no FFR measurement were excluded. For the CT evaluation, vessels with <50% stenosis or CT-FFR >0.80 were regarded as nonsignificant, whereas vessels with 50% to 99% stenosis and CT-FFR ≤0.80, or a total occlusion on CTA, were regarded as having hemodynamically significant CAD. Patients with at least 1 significantly diseased vessel were classified as positive while a negative per-patient classification required normal findings in all 3 vessels. Diagnostic performance was also compared between subgroups stratified by calcium scores <100, 100 to 400, and >400. CTA images quality was scored on a 4-point Likert scale, and diagnostic performance was compared after dividing patients in tertiles of low, intermediate, and high image quality.

Statistical analyses were performed using SPSS (version 21, IBM Corp, Armonk, NY). MedCalc (version 13.0; MedCalc Software, Ostend, Belgium) was used to compare the area under curves.

RESULTS

In total, 351 patients and 525 vessels with direct invasive FFR comparison were available for analysis.

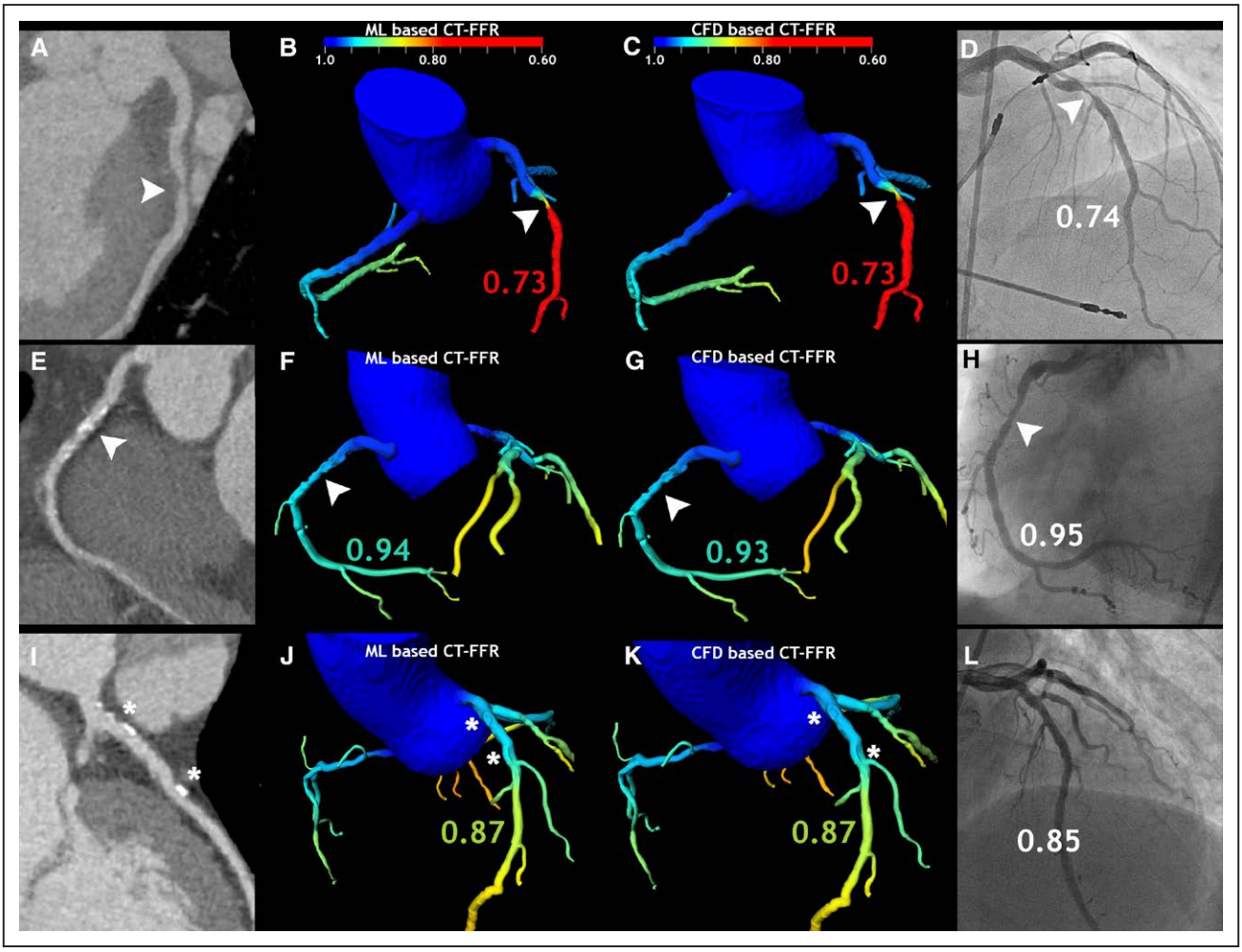

Figure 2. Case example.
Two patients both with moderate (>50%) stenosis (arrow heads) and 1 patient with 2 serial mild stenoses (25%–49% indicated with an asterisk [*]) on CTA (computed tomographic angiography; **A**, **E**, and **I**). In the first patient (**A**–**D**), machine-learning (ML)–based CT-fractional flow reserve (FFR) predicts functionally obstructive stenosis in the mid LAD with a ML-based CT-FFR value of 0.73 (**B**). Computational fluid dynamics (CFD)–based CT-FFR provided an identical result with a CT-FFR value of 0.73. Invasive angiography confirmed functionally obstructive stenosis with an invasive FFR of 0.74 (**D**). In the second patient (**E**–**H**), ML-based CT-FFR predicts the stenosis in the proximal right coronary artery as nonsignificant with a ML-based CT-FFR value of 0.94 (**E**). Invasive angiography (**H**) shows the stenosis. However, invasive FFR confirmed nonfunctionally obstructive stenosis with an invasive FFR of 0.95. In the third patient (**I**–**L**), the 2 serial mild stenoses in the LAD are predicted as nonsignificant with both ML- and CFD-based CT-FFR. Invasive FFR confirmed the nonfunctionally of the lesions with an invasive FFR of 0.85. LAD indicates left anterior descending artery.

Hemodynamically significant disease (invasive FFR ≤0.80) was present in 212 vessels (40%). On CTA, >50% stenosis was present in 382 vessels (73%). ML- and CFD-based CT-FFR classified 245 (47%) and 249 (47%) vessels as functionally obstructed, respectively (Figure 2). Correlation between ML-based and CFD-based CT-FFR was excellent (Pearson R=0.997; Figure I in the Data Supplement). Correlation between

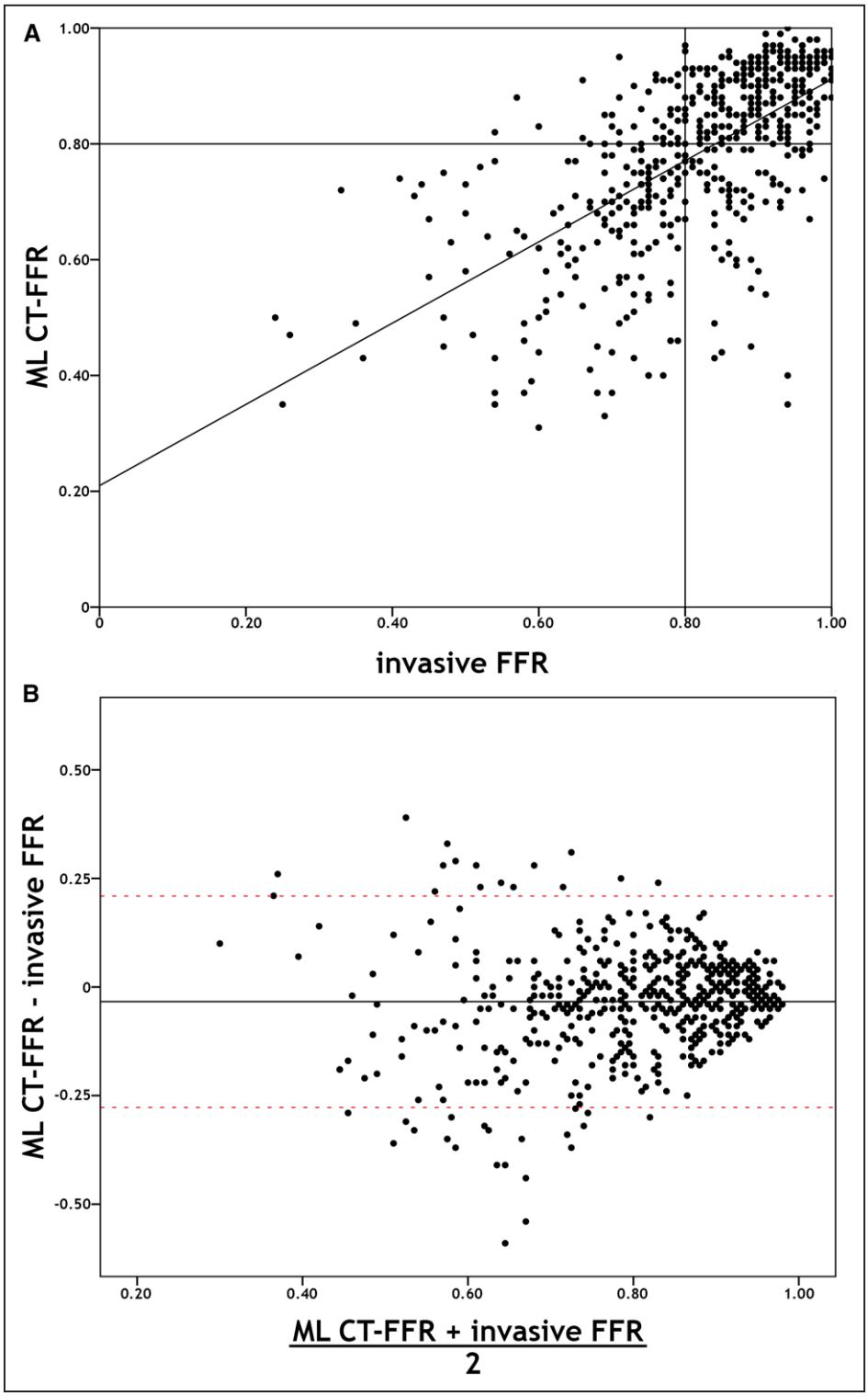

Figure 3. Machine-learning (ML) computed tomography-fractional flow reserve (CT-FFR) and invasive FFR.
A, Scatterplot of 525 vessels compares ML-based CT-FFR with invasive FFR measurements. The Pearson coefficient between ML CT-FFR and invasive FFR was 0.62. **B**, Bland-Altman plot for ML-based CT-FFR and invasive FFR. A horizontal line is placed at the mean difference between ML CT-FFR and invasive FFR (–0.03). The **upper** and **lower** borders of the 95% confidence interval are indicated by the red dotted lines (0.21 and –0.27).

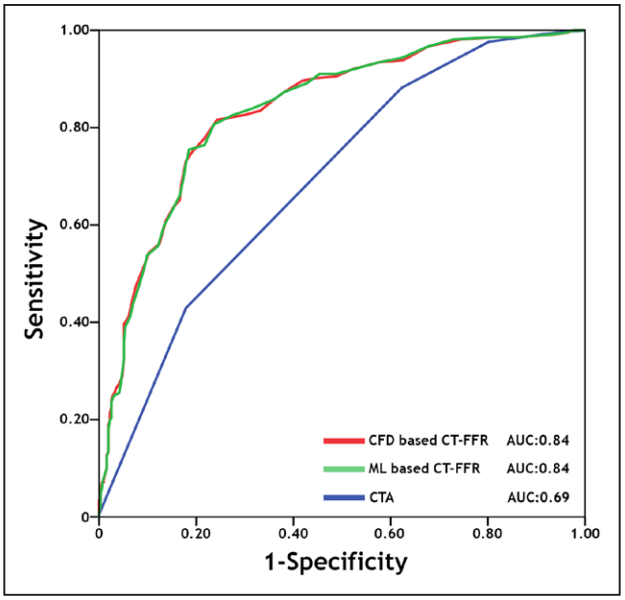

Figure 4. Receiver operating characteristics curve.
Receiver operating characteristics curve, displaying the diagnostic performance of machine-learning (ML) and computational fluid dynamics (CFD)–based computed tomography-fractional flow reserve (CT-FFR) and CT angiography (CTA) in 525 vessels, validated against invasive FFR applying a threshold of ≤0.80 for functional significance. The area under the curve for ML-based CT-FFR was 0.84 (95% confidence interval [CI], 0.80–0.87), identical 0.84 (0.80–0.87) for CFD-based CT-FFR, and 0.69 (0.65–0.74) for CTA. The differences between both ML- and CFD-based CT-FFR and CTA were significant (P<0.0001 for both). AUC indicates area under curve.

ML-based CT-FFR and invasive FFR was moderate (R=0.62; Figure 3A), with an average underestimation of 0.034±0.12 (Figure 3B). The area under the receiver operating characteristic curve for both ML-based (0.84; 95% CI, 0.80–0.87) and CFD-based CT-FFR (0.84; CI, 0.80–0.87) exceeded that of visually classified CTA (0.69; CI, 0.65–0.74; P<0.001 for both ML and CFD; Figure 4).

On a per-vessel basis, ML-based CT-FFR significantly improved specificity, positive predictive value, and accuracy in comparison to CTA (>50% stenosis). When compared with CTA using a threshold of >70% stenosis, sensitivity, negative predictive value, and accuracy improved with ML-based CT-FFR. No significant differences were found between ML- and CFD-based CT-FFR (Table 3). In Figure 5, the diagnostic accuracy of ML-based CT-FFR is shown per invasive FFR interval. In general, a trend of reduced accuracy for values closer to the invasive FFR threshold (0.80) was observed.

Patient-Level Performance

Forty-eight patients had a stenosis in at least 1 coronary artery of 50% to 90% at ICA without an invasive FFR measurement, lacking sufficient information to classify functional significance, leaving 303 patients (86%) for the patient-level analysis. In this clinical, selected cohort where (positive) CTA results contributed to ICA referral, there was a high prevalence of >50% CAD by CTA (96%). The low number of true negative CTAs (n=10), resulted in a low specificity (11%), however, the negative predictive value of CTA remained good (77%). Both positive predictive value (89%) and overall diagnostic accuracy (85%) improved by adding ML-based CT-FFR (Table 4). Of the 85 false-positive CTA results, 62 (73%) could be correctly reclassified based on a normal ML-based CT-FFR result. No differences were found between the different calcium score subgroups. The diagnostic accuracy and negative predictive value of ML-based CT-FFR were significantly larger for the tertile with the highest image quality compared with the tertile with the lowest image quality.

DISCUSSION

The main findings of this article are (1) ML-based CT-FFR closely reproduces CFD-based CT-FFR calculations. (2) In a large population, ML-based CT-FFR correlates moderately with invasive FFR results and correctly reclassifies a substantial proportion of patients with angiographic CAD on CTA. (3) Diagnostic performance of ML-based CT-FFR increases with better image quality, confirming optimization of image quality remains important.

ML techniques are increasingly applied for a variety of medical interests,[21,22,32,33] such as the prediction of carotid artery plaque growth.[23] In cardiovascular medicine, ML models combining quantitative measurements from imaging modalities and clinical features have been used to predict mortality after CTA[18] or early revascularization after SPECT imaging.[20] For the prediction of hemodynamic significance of coronary disease from anatomic CT images, the most important advantage of

Table 3. Per-Vessel Diagnostic Performance

	Sensitivity	Specificity	PPV	NPV	Accuracy
CTA (50% stenosis)	88% (83%–93%)	38% (32%–44%)	49% (44%–54%)	83% (75%–90%)	58% (54%–63%)
CTA (70% stenosis)	43% (38%–50%)	82% (78%–87%)	62% (54%–70%)	68% (63%–73%)	66% (62%–71%)
ML-based CT-FFR	81% (75%–86%)	76% (71%–81%)	70% (64%–76%)	85% (81%–90%)	78% (75%–82%)
CFD-based CT-FFR	82% (77%–87%)	76% (71%–81%)	70% (64%–75%)	86% (82%–90%)	78% (75%–82%)

Vessel-based diagnostic performance of ML- and CFD-based CT-FFR, and CTA, compared with invasive FFR and a threshold of ≤0.80 (n=212) in 525 vessels. CFD indicates computational fluid dynamics; CTA, computed tomography angiography; FFR, fractional flow reserve; ML, machine-learning; NPV, negative predictive value; and PPV, positive predictive value.

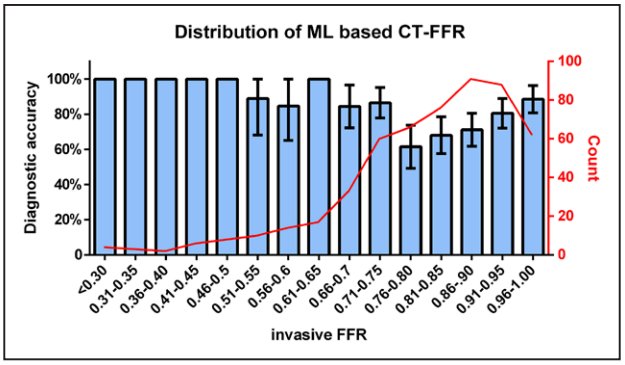

Figure 5. Distribution of machine-learning (ML)–based computed tomography-fractional flow reserve (CT-FFR) accuracy.
Per-vessel diagnostic accuracy with 95% confidence intervals of ML-based CT-FFR, distributed over 0.05 invasive FFR intervals. On the right *y* axis in red, the frequency (count) of a vessel with an invasive FFR value corresponding to each interval. A general trend toward reduced accuracy for values close to the diagnostic threshold of 0.80 for invasive FFR can be observed. In several of the intervals, the sample size is small leading to an accuracy of 100% where no CIs could be computed.

the ML-based approach is the short processing time. Although processing times of CFD algorithms vary with their complexity, from 10 minutes to several hours, ML-based CT-FFR calculations can be performed virtually without delay. Short calculation times allow for interactive interpretation by physicians and the ability to instantaneously observe the effect of adapted vessel segmentation on FFR results. In an independent cohort, consisting of data from 5 centers, we observed that ML-based CT-FFR values correlated near perfectly with CFD-based calculations.

Although coronary CTA allows for effective exclusion of CAD in populations with a lower prevalence of disease, the technique does not allow for accurate interpretation of hemodynamic severity of angiographic lesions. An increasing number of computational solutions have been developed for CTA to assess the degree of flow limitation. In this study, we found as expected a decrease in diagnostic accuracy as the reference measurement (invasive FFR) is approaching to the diagnostic threshold (Figure 5). In this study, the prevalence of physiologically intermediate stenoses (invasive FFR, 0.70–0.80) was 25.5% (134/525), higher than the 12.8% in the meta-analysis by Cook et al.[34] Two hundred ninety-nine of the 525 vessels (57.0%) had an invasive FFR between 0.70 and 0.90. The most extensively validated CT-FFR application is a full-order off-site performed CFD algorithm. The accuracy of this CT-FFR solution to differentiate functionally significant coronary disease was demonstrated in several multicenter, prospective trials.[8–10] Several alternative, on-site performed, CFD-based CT-FFR algorithms have been developed over the past few years with promising results in single-center settings.[12–17] To our knowledge, this is the largest validation study of an on-site CT-FFR application. Using invasive FFR as reference, ML CT-FFR improved the specificity, positive predictive value, and accuracy of CTA. Application of CT-FFR in conjunction with CTA can avoid unnecessary invasive procedures.[35] The ML-based CT-FFR application in this study correctly excluded hemodynamic significance in the majority of >50% stenosis by CTA with an invasive FFR >0.80. Although there are various alternative techniques to assess myocardial ischemia, CT-FFR seems an effective first step after a positive CTA, which does not require further testing or expose to radiation or contrast media.[36] Lu et al[37] showed that off-site CT-FFR was better at predicting

Table 4. Per-Patient Diagnostic Performance

	Sensitivity	Specificity	PPV	NPV	Accuracy
CTA (n=303)	99% (97%–100%)	11% (4%–17%)	71% (65%–76%)	77% (54%–100%)	71% (66%–76%)
CAC <100 (n=102)	97% (90%–100%)	12% (4%–26%)	65% (63%–68%)	71% (34%–92%)	65% (55%–74%)
CAC 100–400 (n=65)	98% (89%–100%)	14% (3%–35%)	72% (67%–75%)	75% (25%–96%)	71% (60%–81%)
CAC >400 (n=108)	99% (95%–100%)	9% (1%–29%)	84% (82%–86%)	67% (16%–96%)	82% (74%–89%)
Lowest image quality (n=101)	96% (91%–100%)	27% (11%–43%)	78% (73%–81%)	73% (46%–99%)	75% (67%–84%)
Intermediate image quality (n=101)	100% (95%–100%)	0% (0%–10%)	72% (63%–81%)	NA NA	72% (64%–81%)
Highest image quality (n=101)	100% (95%–100%)	0% (0%–10%)	65% (56%–75%)	NA NA	67% (56%–75%)
CTA and ML-based CT-FFR (n=303)	89% (85%–94%)	76% (67%–85%)	89% (85%–93%)	77% (68%–85%)	85% (81%–89%)
CAC <100 (n=102)	86% (77%–94%)	80% (68%–93%)	87% (79%–95%)	78% (65%–91%)	83% (76%–91%)
CAC 100–400 (n=65)	93% (86%–100%)	81% (64%–98%)	91% (83%–99%)	80% (69%–100%)	89% (82%–97%)
CAC >400 (n=108)	91% (85%–97%)	71% (52%–91%)	93% (88%–98%)	65% (46%–85%)	87% (81%–93%)
Lowest image quality (n=101)	82% (73%–90%)	60% (43%–78%)	83% (74%–92%)	58% (41%–75%)	75% (67%–83%)
Intermediate image quality (n=101)	92% (85%–98%)	83% (70%–97%)	93% (87%–99%)	81% (67%–95%)	89% (83%–95%)
Highest image quality (n=101)	96% (90%–100%)	83% (70%–95%)	91% (85%–98%)	91% (81%–100%)	91% (86%–97%)

Patient-level diagnostic performance in 303 patients after exclusion of 48 patients because of insufficient information on the functional severity of one of the coronary arteries. In 28 of the 303 patients, no calcium scan was made, as such 275 patients were divided into 3 CAC groups, CAC <100 (n=102), between 100 and 400 (n=65), and >400 (n=108). CAC indicates coronary artery calcium score; CTA, computed tomography angiography; FFR, fractional flow reserve; ML, machine-learning; NPV, negative predictive value; and PPV, positive predictive value.

MACE events than 70% lumen narrowing on CTA, indicating a potential role for CT-FFR in risk assessment. In the 1-year outcomes of the PLATFORM study (Prospective Longitudinal Trial of FFRCT: Outcome and Resource Impacts), off-site CT-FFR guide care resulted in lower costs compared with standard care.[38]

Because CT-FFR depends on an accurate 3D coronary model, image quality is important. Previous studies investigated the relationship between image quality and CT-FFR diagnostic performance and showed that misalignment artifacts negatively affect CT-FFR performance.[25,39,40] In this study, we observed that low image quality had a negative effect of on diagnostic performance. No significance difference in diagnostic accuracy was found for different calcium score subgroups.

Limitations

Based on the original study designs, there was some variation in patient selection and study methodology between the respective cohorts (Table 1). Most patients in this study underwent CTA and invasive FFR for clinical reasons, which resulted in a selection toward a relatively high angiographic and functional coronary disease burden. In total, 65 (16%) patients were excluded, of which 34 because of insufficient CTA image quality. The per-vessel evaluation was based on vessels examined by invasive FFR; however, inclusions of vessels without direct FFR measurement were necessary for the per-patient analysis. It is possible that a proportion of vessels with diffuse disease, but overall <50% diameter narrowing, resulted in myocardial ischemia.[41–45] In a subset of 53 patients, no nitroglycerin was administrated before the CTA, possibly influencing the CT-FFR outcome. The ML-based CT-FFR algorithm investigated in this study is currently available for research purposes.

Conclusions

Without performing individual CFD simulations, on-site CT-FFR based on ML allows for assessment of the hemodynamic severity of coronary stenosis. Both on a per-vessel and per-patient level, the diagnostic accuracy and positive predictive value of CTA can be improved by adding ML-based CT-FFR. Optimization of image quality remain important.

ARTICLE INFORMATION

Received October 12, 2017; accepted April 25, 2018.

The Data Supplement is available at http://circimaging.ahajournals.org/lookup/suppl/doi:10.1161/CIRCIMAGING.117.007217/-/DC1.

Correspondence

Adriaan Coenen, MD, Department of Cardiology, Erasmus University Medical Center, Room Ca-207, 's-Gravendijkwal 230, Rotterdam 3015 CE, the Netherlands. E-mail a.coenen@erasmusmc.nl

Affiliations

Department of Cardiology (A.C., M.L.L., J.D., K.N.) and Department of Radiology (A.C., A.K., M.L.L., K.N.), Erasmus University Medical Center, Rotterdam, the Netherlands. Department of Cardiology, Heart Institute (Y.-H.K.) and Department of Radiology (D.H.Y.), Asan Medical Center, University of Ulsan College of Medicine, Seoul, Korea. Coronary Disease and Structural Heart Diseases Department, Institute of Cardiology, Warsaw, Poland (M.K., C.K.). Division of Cardiovascular Imaging, Medical University of South Carolina, Charleston (C.T., U.J.S.). Department of Radiology and Department of Medical and Health Sciences, Center for Medical Image Science and Visualization, Linköping University, Sweden (J.D.G., A.P.). Department of Radiology, Ehime University Graduate School of Medicine, Japan (A.K.). Corporate Technology, Siemens SRL, Brasov, Romania (L.I.). Medical Imaging Technologies, Siemens Healthcare, Princeton, NJ (S.R., P.S.). Computed Tomography-Research & Development, Siemens Healthcare GmbH, Forchheim, Germany (C.S.). Stanford University School of Medicine, Cardiovascular Institute, Stanford, CA, USA (K.N.).

Sources of Funding

Drs Coenen, Lubbers, and Nieman were supported by a grant from the Dutch Heart Foundation (NHS 2014T061).

Disclosures

Dr Daemen received institutional research support from Acist medical and St Jude Medical. Dr Itu is an employee of Siemens SRL. Drs Rapaka and Sharma are employees of Siemens Medical Solutions USA. C. Schwemmer is an employee of Siemens Healthcare GmbH. Dr Schoepf received institutional research support from Astellas, Bayer Healthcare, GE Healthcare, Siemens Healthineers and consultancy fees from Bayer Healthcare and Guerbet Inc. Dr Nieman received institutional research support from Bayer Healthcare, GE Healthcare, Siemens Medical Solutions, and HeartFlow. The other authors report no conflicts.

REFERENCES

1. Budoff Dowe D, Jollis JG, Gitter M, Sutherland J, Halamert E, Scherer M, Bellinger R, Martin A, Benton R, Delago A, Min JK. Diagnostic performance of 64-multidetector row coronary computed tomographic angiography for evaluation of coronary artery stenosis in individuals without known coronary artery disease: results from the prospective multicenter ACCURACY (Assessment by Coronary Computed Tomographic Angiography of Individuals Undergoing Invasive Coronary Angiography) trial. *J Am Coll Cardiol*. 2008;52:1724–1732.
2. Miller JM, Rochitte CE, Dewey M, Arbab-Zadeh A, Niinuma H, Gottlieb I, Paul N, Clouse ME, Shapiro EP, Hoe J, Lardo AC, Bush DE, de Roos A, Cox C, Brinker J, Lima JA. Diagnostic performance of coronary angiography by 64-row CT. *N Engl J Med*. 2008;359:2324–2336. doi: 10.1056/NEJMoa0806576.
3. Montalescot G, Sechtem U, Achenbach S, Andreotti F, Arden C, Budaj A, Bugiardini R, Crea F, Cuisset T, Di Mario C, Ferreira JR, Gersh BJ, Gitt AK, Hulot JS, Marx N, Opie LH, Pfisterer M, Prescott E, Ruschitzka F, Sabaté M, Senior R, Taggart DP, van der Wall EE, Vrints CJ, Zamorano JL, Achenbach S, Baumgartner H, Bax JJ, Bueno H, Dean V, Deaton C, Erol C, Fagard R, Ferrari R, Hasdai D, Hoes AW, Kirchhof P, Knuuti J, Kolh P, Lancellotti P, Linhart A, Nihoyannopoulos P, Piepoli MF, Ponikowski P, Sirnes PA, Tamargo JL, Tendera M, Torbicki A, Wijns W, Windecker S, Knuuti J, Valgimigli M, Bueno H, Claeys MJ, Donner-Banzhoff N, Erol C, Frank H, Funck-Brentano C, Gaemperli O, Gonzalez-Juanatey JR, Hamilos M, Hasdai D, Husted S, James SK, Kervinen K, Kolh P, Kristensen SD, Lancellotti P, Maggioni AP, Piepoli MF, Pries AR, Romeo F, Rydén L, Simoons ML, Sirnes PA, Steg PG, Timmis A, Wijns W, Windecker S, Yildirir A, Zamorano JL; Task Force Members; ESC Committee for Practice Guidelines; Document Reviewers. 2013 ESC guidelines on the management of stable coronary artery disease: the Task Force on the management of stable coronary artery disease of the European Society of Cardiology. *Eur Heart J*. 2013;34:2949–3003. doi: 10.1093/eurheartj/eht296.
4. Mark DB, Berman DS, Budoff MJ, Carr JJ, Gerber TC, Hecht HS, Hlatky MA, Hodgson JM, Lauer MS, Miller JM, Morin RL, Mukherjee D, Poon M, Rubin GD, Schwartz RS; American College of Cardiology Foundation Task Force on Expert Consensus D. ACCF/ACR/AHA/NASCI/SAIP/SCAI/SCCT 2010 expert consensus document on coronary computed tomographic angiography: a report of the American College of Cardiology Foundation Task Force on Expert Consensus Documents. *J Am Coll Cardiol*. 2010;55:2663–2699. doi: 10.1016/j.jacc.2009.11.013.

5. De Bruyne B, Pijls NH, Kalesan B, Barbato E, Tonino PA, Piroth Z, Jagic N, Möbius-Winkler S, Mobius-Winckler S, Rioufol G, Witt N, Kala P, MacCarthy P, Engström T, Oldroyd KG, Mavromatis K, Manoharan G, Verlee P, Frobert O, Curzen N, Johnson JB, Jüni P, Fearon WF; FAME 2 Trial Investigators. Fractional flow reserve-guided PCI versus medical therapy in stable coronary disease. *N Engl J Med*. 2012;367:991–1001. doi: 10.1056/NEJMoa1205361.
6. Fihn SD, Blankenship JC, Alexander KP, Bittl JA, Byrne JG, Fletcher BJ, Fonarow GC, Lange RA, Levine GN, Maddox TM, Naidu SS, Ohman EM, Smith PK. 2014 ACC/AHA/AATS/PCNA/SCAI/STS focused update of the guideline for the diagnosis and management of patients with stable ischemic heart disease: a report of the American College of Cardiology/American Heart Association Task Force on Practice Guidelines, and the American Association for Thoracic Surgery, Preventive Cardiovascular Nurses Association, Society for Cardiovascular Angiography and Interventions, and Society of Thoracic Surgeons. *J Am Coll Cardiol*. 2014;64:1929–1949. doi: 10.1016/j.jacc.2014.07.017.
7. Taylor CA, Fonte TA, Min JK. Computational fluid dynamics applied to cardiac computed tomography for noninvasive quantification of fractional flow reserve: scientific basis. *J Am Coll Cardiol*. 2013;61:2233–2241. doi: 10.1016/j.jacc.2012.11.083.
8. Koo BK, Erglis A, Doh JH, Daniels DV, Jegere S, Kim HS, Dunning A, DeFrance T, Lansky A, Leipsic J, Min JK. Diagnosis of ischemia-causing coronary stenoses by noninvasive fractional flow reserve computed from coronary computed tomographic angiograms. Results from the prospective multicenter DISCOVER-FLOW (Diagnosis of Ischemia-Causing Stenoses Obtained Via Noninvasive Fractional Flow Reserve) study. *J Am Coll Cardiol*. 2011;58:1989–1997. doi: 10.1016/j.jacc.2011.06.066.
9. Min JK, Leipsic J, Pencina MJ, Berman DS, Koo BK, van Mieghem C, Erglis A, Lin FY, Dunning AM, Apruzzese P, Budoff MJ, Cole JH, Jaffer FA, Leon MB, Malpeso J, Mancini GB, Park SJ, Schwartz RS, Shaw LJ, Mauri L. Diagnostic accuracy of fractional flow reserve from anatomic CT angiography. *JAMA*. 2012;308:1237–1245. doi: 10.1001/2012.jama.11274.
10. Nørgaard BL, Leipsic J, Gaur S, Seneviratne S, Ko BS, Ito H, Jensen JM, Mauri L, De Bruyne B, Bezerra H, Osawa K, Marwan M, Naber C, Erglis A, Park SJ, Christiansen EH, Kaltoft A, Lassen JF, Bøtker HE, Achenbach S; NXT Trial Study Group. Diagnostic performance of noninvasive fractional flow reserve derived from coronary computed tomography angiography in suspected coronary artery disease: the NXT trial (Analysis of Coronary Blood Flow Using CT Angiography: Next Steps). *J Am Coll Cardiol*. 2014;63:1145–1155. doi: 10.1016/j.jacc.2013.11.043.
11. Gaur S, Taylor CA, Jensen JM, Botker HE, Christiansen EH, Kaltoft AK, Holm NR, Leipsic J, Zarins CK, Achenbach S, Khem S, Wilk A, Bezerra HG, Lassen JF, Norgaard BL. FFR derived from coronary CT angiography in nonculprit lesions of patients with recent STEMI. *JACC Cardiovasc Imaging*. 2017;10:424–433.
12. Coenen A, Lubbers MM, Kurata A, Kono A, Dedic A, Chelu RG, Dijkshoorn ML, Gijsen FJ, Ouhlous M, van Geuns RJ, Nieman K. Fractional flow reserve computed from noninvasive CT angiography data: diagnostic performance of an on-site clinician-operated computational fluid dynamics algorithm. *Radiology*. 2015;274:674–683. doi: 10.1148/radiol.14140992.
13. Renker M, Schoepf UJ, Wang R, Meinel FG, Rier JD, Bayer RR II, Möllmann H, Hamm CW, Steinberg DH, Baumann S. Comparison of diagnostic value of a novel noninvasive coronary computed tomography angiography method versus standard coronary angiography for assessing fractional flow reserve. *Am J Cardiol*. 2014;114:1303–1308. doi: 10.1016/j.amjcard.2014.07.064.
14. Kruk M, Wardziak Ł, Demkow M, Pleban W, Pręgowski J, Dzielińska Z, Witulski M, Witkowski A, Rużyłło W, Kępka C. Workstation-based calculation of CTA-based FFR for intermediate stenosis. *JACC Cardiovasc Imaging*. 2016;9:690–699. doi: 10.1016/j.jcmg.2015.09.019.
15. De Geer J, Sandstedt M, Björkholm A, Alfredsson J, Janzon M, Engvall J, Persson A. Software-based on-site estimation of fractional flow reserve using standard coronary CT angiography data. *Acta Radiol*. 2016;57:1186–1192. doi: 10.1177/0284185115622075.
16. Yang DH, Kim YH, Roh JH, Kang JW, Ahn JM, Kweon J, Lee JB, Choi SH, Shin ES, Park DW, Kang SJ, Lee SW, Lee CW, Park SW, Park SJ, Lim TH. Diagnostic performance of on-site CT-derived fractional flow reserve versus CT perfusion. *Eur Heart J Cardiovasc Imaging*. 2016;18:432–440.
17. Ko BS, Cameron JD, Munnur RK, Wong DTL, Fujisawa Y, Sakaguchi T, Hirohata K, Hislop-Jambrich J, Fujimoto S, Takamura K, Crossett M, Leung M, Kuganesan A, Malaiapan Y, Nasis A, Troupis J, Meredith IT, Seneviratne SK. Noninvasive CT-derived FFR based on structural and fluid analysis: a comparison with invasive FFR for detection of functionally significant stenosis. *JACC Cardiovascular Imaging*. 2017;10:663–673.
18. Motwani M, Dey D, Berman DS, Germano G, Achenbach S, Al-Mallah MH, Andreini D, Budoff MJ, Cademartiri F, Callister TQ, Chang HJ, Chinnaiyan K, Chow BJ, Cury RC, Delago A, Gomez M, Gransar H, Hadamitzky M, Hausleiter J, Hindoyan N, Feuchtner G, Kaufmann PA, Kim YJ, Leipsic J, Lin FY, Maffei E, Marques H, Pontone G, Raff G, Rubinshtein R, Shaw LJ, Stehli J, Villines TC, Dunning A, Min JK, Slomka PJ. Machine learning for prediction of all-cause mortality in patients with suspected coronary artery disease: a 5-year multicentre prospective registry analysis. *Eur Heart J*. 2017;38:500–507.
19. Arsanjani R, Xu Y, Dey D, Vahistha V, Shalev A, Nakanishi R, Hayes S, Fish M, Berman D, Germano G, Slomka PJ. Improved accuracy of myocardial perfusion SPECT for detection of coronary artery disease by machine learning in a large population. *J Nucl Cardiol*. 2013;20:553–562. doi: 10.1007/s12350-013-9706-2.
20. Arsanjani R, Dey D, Khachatryan T, Shalev A, Hayes SW, Fish M, Nakanishi R, Germano G, Berman DS, Slomka P. Prediction of revascularization after myocardial perfusion SPECT by machine learning in a large population. *J Nucl Cardiol*. 2015;22:877–884. doi: 10.1007/s12350-014-0027-x.
21. Parmar C, Grossmann P, Bussink J, Lambin P, Aerts HJ. Machine learning methods for Quantitative Radiomic Biomarkers. *Sci Rep*. 2015;5:13087. doi: 10.1038/srep13087.
22. Obermeyer Z, Emanuel EJ. Predicting the future—big data, machine learning, and clinical medicine. *N Engl J Med*. 2016;375:1216–1219. doi: 10.1056/NEJMp1606181.
23. van Engelen A, Wannarong T, Parraga G, Niessen WJ, Fenster A, Spence JD, de Bruijne M. Three-dimensional carotid ultrasound plaque texture predicts vascular events. *Stroke*. 2014;45:2695–2701. doi: 10.1161/STROKEAHA.114.005752.
24. Narula S, Shameer K, Salem Omar AM, Dudley JT, Sengupta PP. Machine-learning algorithms to automate morphological and functional assessments in 2D echocardiography. *J Am Coll Cardiol*. 2016;68:2287–2295. doi: 10.1016/j.jacc.2016.08.062.
25. Coenen A, Lubbers MM, Kurata A, Kono A, Dedic A, Chelu RG, Dijkshoorn ML, van Geuns RJ, Schoebinger M, Itu L, Sharma P, Nieman K. Coronary CT angiography derived fractional flow reserve: methodology and evaluation of a point of care algorithm. *J Cardiovasc Comput Tomogr*. 2016;10:105–113. doi: 10.1016/j.jcct.2015.12.006.
26. Raff GL, Abidov A, Achenbach S, Berman DS, Boxt LM, Budoff MJ, Cheng V, DeFrance T, Hellinger JC, Karlsberg RP; Society of Cardiovascular Computed Tomography. SCCT guidelines for the interpretation and reporting of coronary computed tomographic angiography. *J Cardiovasc Comput Tomogr*. 2009;3:122–136. doi: 10.1016/j.jcct.2009.01.001.
27. Itu L, Sharma P, Mihalef V, Kamen A, Suciu C, Lomaniciu D. A patient-specific reduced-order model for coronary circulation. *2012 9th IEEE International Symposium on Biomedical Imaging (ISBI)*. 2012:832–835.
28. Wilson RF, Wyche K, Christensen BV, Zimmer S, Laxson DD. Effects of adenosine on human coronary arterial circulation. *Circulation*. 1990;82:1595–1606.
29. Itu L, Rapaka S, Passerini T, Georgescu B, Schwemmer C, Schoebinger M, Flohr T, Sharma P, Comaniciu D. A machine-learning approach for computation of fractional flow reserve from coronary computed tomography. *J Appl Physiol (1985)*. 2016;121:42–52. doi: 10.1152/japplphysiol.00752.2015.
30. DeLong ER, DeLong DM, Clarke-Pearson DL. Comparing the areas under two or more correlated receiver operating characteristic curves: a nonparametric approach. *Biometrics*. 1988;44:837–845.
31. Genders TS, Spronk S, Stijnen T, Steyerberg EW, Lesaffre E, Hunink MG. Methods for calculating sensitivity and specificity of clustered data: a tutorial. *Radiology*. 2012;265:910–916. doi: 10.1148/radiol.12120509.
32. de Bruijne M. Machine learning approaches in medical image analysis: from detection to diagnosis. *Med Image Anal*. 2016;33:94–97. doi: 10.1016/j.media.2016.06.032.
33. Gulshan V, Peng L, Coram M, Stumpe MC, Wu D, Narayanaswamy A, Venugopalan S, Widner K, Madams T, Cuadros J, Kim R, Raman R, Nelson PC, Mega JL, Webster DR. Development and validation of a deep learning algorithm for detection of diabetic retinopathy in retinal fundus photographs. *JAMA*. 2016;316:2402–2410. doi: 10.1001/jama.2016.17216.
34. Cook CM, Petraco R, Shun-Shin MJ, Ahmad Y, Nijjer S, Al-Lamee R, Kikuta Y, Shiono Y, Mayet J, Francis DP, Sen S, Davies JE. Diagnostic accuracy of computed tomography-derived fractional flow reserve: a systematic review. *JAMA Cardiol*. 2017;2:803–810. doi: 10.1001/jamacardio.2017.1314.
35. Douglas PS, Pontone G, Hlatky MA, Patel MR, Norgaard BL, Byrne RA, Curzen N, Purcell I, Gutberlet M, Rioufol G, Hink U, Schuchlenz HW,

Feuchtner G, Gilard M, Andreini D, Jensen JM, Hadamitzky M, Chiswell K, Cyr D, Wilk A, Wang F, Rogers C, De Bruyne B; PLATFORM Investigators. Clinical outcomes of fractional flow reserve by computed tomographic angiography-guided diagnostic strategies vs. usual care in patients with suspected coronary artery disease: the prospective longitudinal trial of FFR(CT): outcome and resource impacts study. *Eur Heart J*. 2015;36:3359–3367. doi: 10.1093/eurheartj/ehv444.

36. Coenen A, Rossi A, Lubbers MM, Kurata A, Kono AK, Chelu RG, Segreto S, Dijkshoorn ML, Wragg A, van Geuns RM, Pugliese F, Nieman K. Integrating CT myocardial perfusion and CT-FFR in the work-up of coronary artery disease. *JACC Cardiovasc Imaging*. 2017;10:760–770. doi: 10.1016/j.jcmg.2016.09.028.
37. Lu MT, Ferencik M, Roberts RS, Lee KL, Ivanov A, Adami E, Mark DB, Jaffer FA, Leipsic JA, Douglas PS, Hoffmann U. Noninvasive FFR derived from coronary CT angiography: management and outcomes in the PROMISE trial. *JACC Cardiovasc Imaging*. 2017;10:1350–1358. doi: 10.1016/j.jcmg.2016.11.024.
38. Douglas PS, De Bruyne B, Pontone G, Patel MR, Norgaard BL, Byrne RA, Curzen N, Purcell I, Gutberlet M, Rioufol G, Hink U, Schuchlenz HW, Feuchtner G, Gilard M, Andreini D, Jensen JM, Hadamitzky M, Chiswell K, Cyr D, Wilk A, Wang F, Rogers C, Hlatky MA; PLATFORM Investigators. 1-year outcomes of FFRCT-guided care in patients with suspected coronary disease: the PLATFORM study. *J Am Coll Cardiol*. 2016;68:435–445. doi: 10.1016/j.jacc.2016.05.057.
39. Min JK, Koo BK, Erglis A, Doh JH, Daniels DV, Jegere S, Kim HS, Dunning A, Defrance T, Leipsic J. Effect of image quality on diagnostic accuracy of noninvasive fractional flow reserve: results from the prospective multicenter international DISCOVER-FLOW study. *J Cardiovasc Comput Tomogr*. 2012;6:191–199. doi: 10.1016/j.jcct.2012.04.010.
40. Leipsic J, Yang TH, Thompson A, Koo BK, Mancini GB, Taylor C, Budoff MJ, Park HB, Berman DS, Min JK. CT angiography (CTA) and diagnostic performance of noninvasive fractional flow reserve: results from the Determination of Fractional Flow Reserve by Anatomic CTA (DeFACTO) study. *AJR Am J Roentgenol*. 2014;202:989–994. doi: 10.2214/AJR.13.11441.
41. Nakazato R, Park HB, Berman DS, Gransar H, Koo BK, Erglis A, Lin FY, Dunning AM, Budoff MJ, Malpeso J, Leipsic J, Min JK. Noninvasive fractional flow reserve derived from computed tomography angiography for coronary lesions of intermediate stenosis severity: results from the DeFACTO study. *Circ Cardiovasc Imaging*. 2013;6:881–889. doi: 10.1161/CIRCIMAGING.113.000297.
42. Bech GJ, De Bruyne B, Pijls NH, de Muinck ED, Hoorntje JC, Escaned J, Stella PR, Boersma E, Bartunek J, Koolen JJ, Wijns W. Fractional flow reserve to determine the appropriateness of angioplasty in moderate coronary stenosis: a randomized trial. *Circulation*. 2001;103:2928–2934.
43. Ahmadi A, Stone GW, Leipsic J, Serruys PW, Shaw L, Hecht H, Wong G, Nørgaard BL, O'Gara PT, Chandrashekhar Y, Narula J. Association of coronary stenosis and plaque morphology with fractional flow reserve and outcomes. *JAMA Cardiol*. 2016;1:350–357. doi: 10.1001/jamacardio.2016.0263.
44. Curzen N, Rana O, Nicholas Z, Golledge P, Zaman A, Oldroyd K, Hanratty C, Banning A, Wheatcroft S, Hobson A, Chitkara K, Hildick-Smith D, McKenzie D, Calver A, Dimitrov BD, Corbett S. Does routine pressure wire assessment influence management strategy at coronary angiography for diagnosis of chest pain?: the RIPCORD study. *Circ Cardiovasc Interv*. 2014;7:248–255. doi: 10.1161/CIRCINTERVENTIONS.113.000978.
45. Tonino PA, Fearon WF, De Bruyne B, Oldroyd KG, Leesar MA, Ver Lee PN, Maccarthy PA, Van't Veer M, Pijls NH. Angiographic versus functional severity of coronary artery stenoses in the FAME study fractional flow reserve versus angiography in multivessel evaluation. *J Am Coll Cardiol*. 2010;55:2816–2821. doi: 10.1016/j.jacc.2009.11.096.

Circulation
Cardiovascular Imaging

Diagnostic Accuracy of a Machine-Learning Approach to Coronary Computed Tomographic Angiography–Based Fractional Flow Reserve: Result From the MACHINE Consortium

Adriaan Coenen, Young-Hak Kim, Mariusz Kruk, Christian Tesche, Jakob De Geer, Akira Kurata, Marisa L. Lubbers, Joost Daemen, Lucian Itu, Saikiran Rapaka, Puneet Sharma, Chris Schwemmer, Anders Persson, U. Joseph Schoepf, Cezary Kepka, Dong Hyun Yang and Koen Nieman

Circ Cardiovasc Imaging. 2018;11:
doi: 10.1161/CIRCIMAGING.117.007217
Circulation: Cardiovascular Imaging is published by the American Heart Association, 7272 Greenville Avenue, Dallas, TX 75231

Print ISSN: 1941-9651. Online ISSN: 1942-0080

SUPPLEMENTAL MATERIAL

Supplemental table 1: 28 features of the machine learning application.

Nr	Feature	Type
1	Distal radius of most significant stenosis upstream	Upstream
2	Minimum radius of most significant stenosis upstream	Upstream
3	Reference radius of branch containing most significant stenosis upstream	Upstream
4	Percentage diameter stenosis of most significant stenosis upstream	Upstream
5	Total length of most significant stenosis upstream	Upstream
6	Minimum radius length of most significant stenosis upstream	Upstream
7	Entrance length of most significant stenosis upstream	Upstream
8	Exit length of most significant stenosis upstream	Upstream
9	Intrinsic ischemic contribution score of most significant stenosis upstream	Upstream
10	Expansion ischemic contribution score of most significant stenosis upstream	Upstream
11	Tapering ischemic contribution score of most significant stenosis upstream	Upstream
12	Total ischemic contribution score of most significant stenosis upstream	Upstream
13	Percentage diameter stenosis of second most significant stenosis upstream	Upstream
14	Total ischemic contribution score of second most significant stenosis upstream	Upstream
15	Percentage diameter stenosis of third most significant stenosis upstream	Upstream
16	Total ischemic contribution score of third most significant stenosis upstream	Upstream
17	Percentage diameter stenosis of fourth most significant stenosis upstream	Upstream
18	Total ischemic contribution score of fourth most significant stenosis upstream	Upstream
19	Percentage diameter stenosis of most significant stenosis downstream	Downstream
20	Total ischemic contribution score of most significant stenosis downstream	Downstream
21	Percentage diameter stenosis of second most significant stenosis downstream	Downstream
22	Total ischemic contribution score of second most significant stenosis downstream	Downstream
23	Aggregated ischemic contribution score between ostium and current location	Upstream - Local
24	Aggregated healthy ischemic contribution score between ostium and current location	Upstream – Local
25	Aggregated ischemic contribution score between current location and largest downstream outlet	Local - downstream
26	Aggregated healthy ischemic contribution score between current location and largest downstream outlet	Local - downstream
27	Ischemic weight of the current coronary segment	Local
28	Left ventricular mass	Global

Supplemental Figure 1

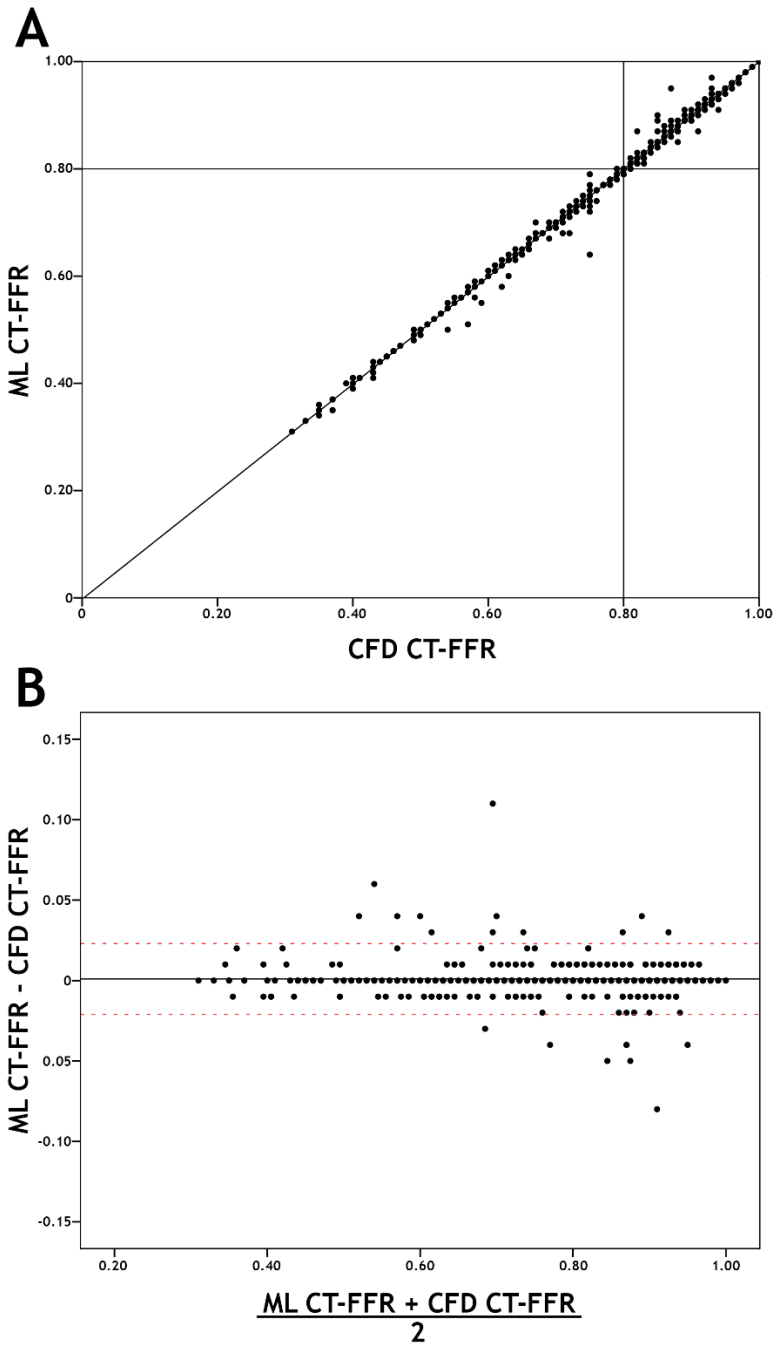

Supplemental figure 1 ML CT-FFR and CFD CT-FFR: In panel A, a scatterplot of 525 vessels compares ML based CT-FFR results with CFD based CT-FFR. The correlation between ML and CFD based CT-FFR was excellent with a Pearson's coefficient of 0.997. Panel B shows the Bland-Altman plot for ML and CFD based CT-FFR. There was a minimal non-relevant mean overestimation of ML CT-FFR over CFD based CT-FFR (0.0009), with small 95% confidence interval (0.02 & -0.02) (red dotted lines).
CFD: computational fluid dynamics, ML: machine-learning